Technical Note

Fast high-resolution LA-ICP-MS imaging of the distribution of platinum-based anti-cancer compounds in multicellular tumor spheroids

Sarah Theiner, Stijn J. M. Van Malderen, Thibaut Van Acker, Anton A. Legin, Bernhard K. Keppler, Frank Vanhaecke, and Gunda Koellensperger

Anal. Chem., **Just Accepted Manuscript** • DOI: 10.1021/acs.analchem.7b02681 • Publication Date (Web): 04 Nov 2017

Fast high-resolution LA-ICP-MS imaging of the distribution of platinum-based anti-cancer compounds in multicellular tumor spheroids

Sarah Theiner[a§], Stijn J. M. Van Malderen[b§], Thibaut Van Acker[b], Anton Legin[c], Bernhard K. Keppler[c,d], Frank Vanhaecke[b], Gunda Koellensperger[a*]

[a] Institute of Analytical Chemistry, University of Vienna, Waehringer Strasse 38, 1090 Vienna, Austria

[b] Department of Analytical Chemistry, Ghent University, Campus Sterre, Krijgslaan 281-S12, 9000 Ghent, Belgium

[c] Institute of Inorganic Chemistry, University of Vienna, Waehringer Strasse 42, 1090 Vienna, Austria

[d] Research Platform 'Translational Cancer Therapy Research', University of Vienna, Waehringer Strasse 42, 1090 Vienna, Austria

[§] These authors contributed equally to this paper.

[*] Corresponding author: Gunda Koellensperger; Institute of Analytical Chemistry, Waehringer Strasse 38, 1090 Vienna, Austria. Tel: +43-1-4277-52303, Email: gunda.koellenspeger@univie.ac.at

Abstract

Multicellular tumor spheroid models serve as an important three-dimensional *in vitro* cell model system as they mimic the complex tumor micro-environment and thus have contributed to valuable assays in drug discovery studies. In this study, we present a state-of-the-art laser ablation-inductively coupled plasma-mass spectrometry (LA-ICP-MS) setup for high spatial resolution elemental imaging of multicellular tumor spheroids and an approach to account for variations in cell density. A low dispersion LA-ICP-MS setup was employed, providing accelerated throughput, high sensitivity and permitting a lateral image resolution down to ~2.5 µm for phosphorus and platinum in HCT116 colon cancer spheroids upon treatment with the clinically used anti-cancer drug oxaliplatin. Phosphorus was introduced as scalar to compensate for differences in cell density and tissue thickness and the Pt/P ratios together with the high resolution adopted in our approach allows the differentiation of platinum accumulation within each part of the morphology of the tumor spheroids (layers of proliferating, quiescent and necrotic cells).

Introduction

High-performance screening approaches, designed to cross out poorly performing compounds in a fast and reliable way in order to prioritize promising drug candidates at an early stage, are in high demand in the pre-clinical drug development process. Such screening approaches would reduce the cost per experiment, permitting larger libraries of compounds to be screened, thus increasing the success rate of drug discovery. During the last decades, 2-dimensional (2D) cell-based assay models, in which cells are exposed to uniform conditions and drug concentrations in an artificial micro-environment are commonly employed for testing the efficacy of anti-cancer drugs.[1] One of the main limiting factors of the effectiveness of cancer therapy in its capability to prevent the recurrence of tumors is the failure of the drug to effectively penetrate into the tumor tissue.[2] In this context, three-dimensional (3D) multicellular tumor spheroids (MCTS) are being increasingly used as advanced *in vitro* systems to evaluate the penetration of the drug into the tumor, thus bridging the gap between 2D cell assays and animal experiments.[3,4] Multicellular tumor spheroids (MCTS) closely resemble *in vivo* avascular tumor nodules in terms of pathophysiological gradients and functional features, providing an excellent platform for probing the distributions of drugs and potential drug candidates.[3] The characterization of tumor spheroids and the assessment of drug distributions in MCTS are essential to establish them as reliable *in vitro* models to test potential drug candidates in a high-throughput manner.[1] Their relatively small size (~200-800 µm in diameter) and heterogeneous morphology raise the need for imaging techniques which can provide a high detection power, selectivity, a linear response to the volumetric concentration, and high spatial resolution for characterizing the anti-cancer drug penetration within each part of the morphology.[5] Imaging techniques including fluorescence imaging, X-ray fluorescence

(XRF) and matrix-assisted laser desorption ionization-mass spectrometry (MALDI-MS) have been used to study the uptake of metal-based anticancer agents into tumor spheroid models.[6-10] Synchrotron-induced-XRF (SR-XRF) is also attractive for elemental imaging; however the detection of low platinum levels in biological samples could be problematic due to the relatively low sensitivity of XRF for platinum compared to other elements. Additionally, the availability of SR-XRF is problematic for routine screening of a large batch of samples for pre-clinical applications.[9] Laser ablation-inductively coupled plasma-mass spectrometry (LA-ICP-MS), an elemental imaging tool, has been demonstrated to offer fast, sensitive, and selective tracking of metal-based chemotherapeutic drugs in MCTS; in a recent study, LA-ICP-MS was used to evaluate the uptake of platinum-based anti-cancer drugs into tumor spheroids at a spatial resolution of ~10 µm.[11-13] However, in order to establish LA-ICP-MS as a viable routine screening tool for clinical applications, further improvements in both lateral resolution and sample throughput are required. A high lateral resolution would allow drug accumulation studies addressing extracellular accumulation within 3D tumor models and more detailed studies in co-culture models. Recently, low dispersion ablation cells have been developed, which enhance the wash-out time up to two orders of magnitude, enabling significantly higher sample throughput, whilst the compression of the aerosol clouds formed upon each single laser impact increases the signal-to-noise ratio, which permits these systems to achieve higher lateral resolutions without compromising the sensitivity.[14,15] Low dispersion cells have already shown their potential for a variety of applications, as reviewed elsewhere.[14] In metal-based anti-cancer drug research, a fast wash-out system has been used to study the platinum distribution at a pixel size of ~ 1 µm in Cynomolgus kidney upon treatment with cisplatin at a clinically relevant dose

inducing kidney lesions[16] and in ovarian cancer xenografts after treatment with cisplatin.[17]

In this study, a low dispersion LA-ICP-MS setup[18] is used to enhance the analysis speed and to enable high-resolution elemental imaging for studying the penetration of metal-based anticancer drugs into colon cancer HCT116 tumor spheroids. Moreover, we aim at introducing the phosphorus signal as compensation for variations in cell density, which allows together with the high spatial resolution of the approach the differentiation of platinum accumulation in areas of proliferating and quiescent cells as well as in the necrotic core.

Experimental

Cell line and cultivation conditions

Human colorectal carcinoma cells (HCT116) were provided by Brigitte Marian (Institute of Cancer Research, Department of Medicine I, Medical University of Vienna, Austria). Cells were grown in Roswell Park Memorial Institute (RPMI) medium supplemented with 10% heat-inactivated fetal bovine serum (Biowest, France) and 4 mM L-glutamine (Sigma Aldrich, Austria) according to standard procedures.[19] Monolayer cell cultures were grown in 75 cm^2 flasks (CytoOne, Starlab, UK) at 37 °C in a moist atmosphere containing 5% CO_2.

Spheroid culture

For spheroid production for LA-ICP-MS imaging, HCT116 cells were harvested from culture flasks by trypsinization and seeded in non-cell culture treated round bottom 96-well plates (VWR, Austria) in densities of 2×10^3 cells per well. 3D cultures were grown seven days (to achieve necrotic core formation) prior to treatment. On day seven, the spheroids were treated for 24 h with 400 µM oxaliplatin (the stock solution was prepared directly in RPMI medium). Oxaliplatin was prepared using standard literature methods as described in Ref. 18.[20] After the treatment, the spheroids were collected, washed three times in PBS, transferred and embedded into gelatin for further sample preparation steps. Tumor spheroids were sectioned with a cryotome into 12 µm thick sections which were deposited onto microscope slides. Based on brightfield images acquired by optical microscopy, sequential sections of HCT116 tumor spheroids with visible concentric rings of heterogeneous cell populations including the necrotic core region were selected for high resolution LA-ICP-MS

analysis. Individual tumor spheroids were controlled under the microscope (Olympus CKX41, Olympus, Austria) and their diameters were measured both in the vertical and horizontal direction by cellF 2.7 imaging software.

High-resolution imaging of tumor spheroids by LA-ICP-MS

An Analyte G2 193 nm ArF* excimer-based laser ablation (LA) system (Teledyne Photon Machines, Bozeman, MT, USA), equipped with a HelEx II 2-volume ablation cell, was coupled to an Agilent 7900 quadrupole-based ICP-MS unit (Agilent Technologies, Waltham, MA, USA) via the aerosol rapid introduction system (ARIS) in order to obtain laterally-resolved images of the distributions of phosphorous and platinum in HCT116 tumor spheroids. The mixing bulb of the ARIS (developed at Ghent University and mean-while commercially available via Teledyne CETAC Technologies) was used to introduce an Ar make-up gas flow (~1.20 L min^{-1}) into the He carrier gas flow (0.60 L min^{-1}) before entering the plasma. Laser ablation sampling was performed according to parallel line scans, at a repetition rate of 50 Hz, with a circular spot size of 5 µm diameter and at a lateral scan speed of 25 µm s^{-1}. The parallel line scans overlapped one another with 2.5 µm to achieve a higher spatial resolution in this direction. NIST SRM 612 glass certified reference material (National Institute for Standards and Technology, Gaithersburg, MD, USA) was used for the daily tuning of the operational parameters of the LA-ICP-MS system for maximum sensitivity for ^{7}Li, ^{115}In and ^{238}U, low oxide formation based on the $^{238}U^{16}O^{+}/^{238}U^{+}$ ratio (<1%) and low laser-induced elemental fractionation based on the $^{238}U^{+}/^{232}Th^{+}$ ratio (~1). The following ICP-MS instrument settings were used: radio frequency power of 1400 W, an auxiliary Ar gas flow rate of ~ 0.90 L min^{-1}, plasma gas flow rate of 15 L min^{-1}. ^{31}P and ^{195}Pt were monitored with dwell times of 15 ms

and 35 ms, respectively. The transient data were processed by a collection of Python 3.4 scripts to produce 2D images. The data processing includes a subtraction of the gas blank and matching the transient MS signal to a virtual grid, retrieved from the laser log files. The aspect ratio of the pixels was calculated to accurately reflect the ablated section, and the image was rendered according to this aspect ratio using the Matplotlib plotting library.

Results and Discussion

Herein, we present the first high-resolution LA-ICP-MS images of phosphorus and platinum in human colon carcinoma HCT116 tumor spheroids using an LA-ICP-MS setup based on the low dispersion mixing bulb ARIS that provides fast aerosol wash-out, high sensitivity and high spatial resolution. Together with an oversampling and image deconvolution approach,[21] a high spatial resolution of ~2.5 µm was obtained for parallel imaging of the distributions of phosphorus and platinum in tumor spheroid cryo-sections. The HCT116 MCTS were treated with oxaliplatin as model compound, which is routinely used in chemotherapy for the treatment of colorectal cancer.[22] The high resolution LA-ICP-MS maps of the phosphorus and platinum accumulation are shown in Figure 1 and 2.

Platinum was observed to accumulate at the periphery of the tumor spheroid, consisting of proliferating cells, which have ample access to nutrients and oxygen. The cells in the outer rim of the spheroid resemble cells in tumors, which are close to the blood vessels.[23] In the design of new platinum-based agents, the optimization of properties to improve cellular uptake can lead to exclusive accumulation in proliferating cells and might reduce the ability of the compound to penetrate deeper into tumor tissue. For oxaliplatin, pronounced platinum accumulation was also found in the necrotic core of the HCT116 tumor spheroids by the use of high-resolution LA-ICP-MS. The presence of a necrotic core in HCT116 tumor spheroids was previously confirmed for MCTS of sizes >400 µm.[24] This result is in accordance with previous investigations by LA-ICP-MS in a murine colon cancer CT-26 model, where it was demonstrated that platinum was also found in necrotic and solid parts of tumor tissue in contrast to experimental compounds.[25] The detection of platinum in the core indicates that after 24 h incubation with oxaliplatin, the drug and/or its metabolites

seem to have penetrated the entire HCT116 spheroid and reached its center. A recent study by MALDI-MS showed the presence of the intact drug oxaliplatin at the outer rim of HCT116 tumor spheroids, in an environment which mimics hyperthermic intraperitoneal chemotherapy-like treatment conditions.[8] In the necrotic core, only oxaliplatin bound to methionine was detected which indicates that the necrotic core might serve as a reservoir for metabolites. The lowest levels of platinum were detected in the middle layer of the tumor spheroid sections which comprises quiescent viable cells. Other imaging studies on platinum(IV) compounds in HCT116 spheroids with LA-ICP-MS[11,12] and on cisplatin in DLD-1 spheroids with X-ray fluorescence computed micro-tomography (XRF-CT)[7] revealed a similar platinum accumulation pattern in the different regions of the MCTS.

However, as the cell density, cell number and protein content varies per investigated area in tumor spheroids, the raw platinum distribution per area may not accurately reflect the dose of platinum within each cell. Hence, it is important to introduce scalars to compensate for these differences and to be able to give the platinum content per cell. Herein, we propose the parallel imaging of phosphorus to account for differences in cell density and tissue thickness. The high-resolution images obtained by LA-ICP-MS show, that the phosphorus accumulation pattern strongly follows the platinum distribution in HCT116 tumor spheroid sections (Figures 1 and 2). Higher levels of phosphorus were detected in the outer rim of proliferating cells and in the necrotic core, compared to the middle layer of the spheroid. Therefore, the tumor spheroid LA-ICP-MS images were segmented into three regions of interest (ROIs) – the necrotic core, the inner layer of quiescent cells and the outer layer of proliferating cells – and the platinum to phosphorus ratios were calculated for each ROI (Figure 3B). The highest Pt/P ratio was obtained for the central region, followed by the outer

rim of the spheroid whereas the lowest ratio was observed in the middle layer (Pt/P ratio of 0.6 ± 0.09, 0.4 ± 0.01 and 0.2 ± 0.03 respectively). The high lateral resolution adopted in our approach permitted to segment the different layers of the spheroid, whilst eliminating the pixels associated with intra-cellular space, *i.e.* regions inside the tumor where no tissue was present (Figure 3B). These pixels were withheld by thresholding the phosphorus signal at a level of 3 times the signal background of the glass substrate. As a result, the model for the penetration depth becomes more accurate, as the effect on the average Pt/P ratio of these 'empty' pixels is negated. By imaging the spheroid at a higher lateral resolution and using the Pt/P ratio, it also became clear that the cell density and platinum accumulation in the necrotic core of the spheroid is very inhomogeneous. The zoomed figure insets in Figures 1 and 2 illustrate these local differences in zones of the core.

An average radial profile was built, which, based on the apparent symmetry of the spheroid morphology, should be representative of the overall drug penetration in the spheroid (Figure 3A). When considering the cumulative Pt/P ratio in the MCTS, approximately 20-25% of the platinum is concentrated in the first 70-80 µm of the outer layer. The intermediary layer, a broader strip of quiescent cells, contributes another 30%, whilst the necrotic core strongly accumulates the drug and/or its metabolites.

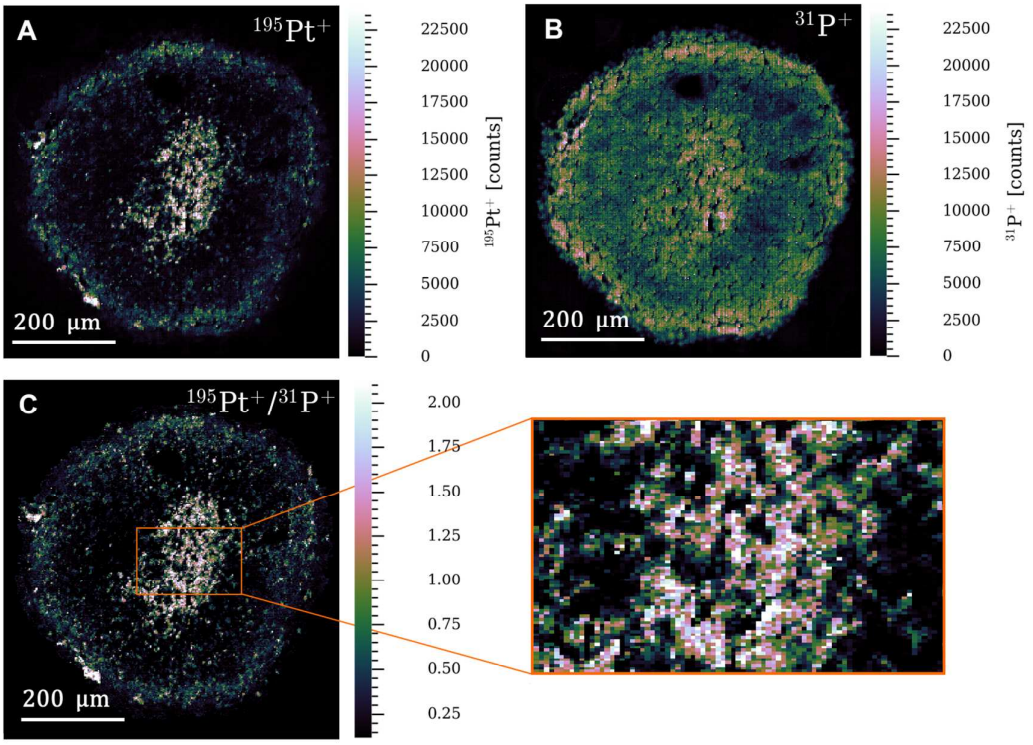

Figure 1. High-resolution LA-ICP-MS images of the (A) ^{195}Pt, (B) ^{31}P and (C) $^{195}Pt^+/^{31}P^+$ signal ratio distribution in a selected colon cancer HCT116 tumor spheroid section 1, after treatment with oxaliplatin for 24 h. The inset of Figure (C) shows a zoomed-in section of the image.

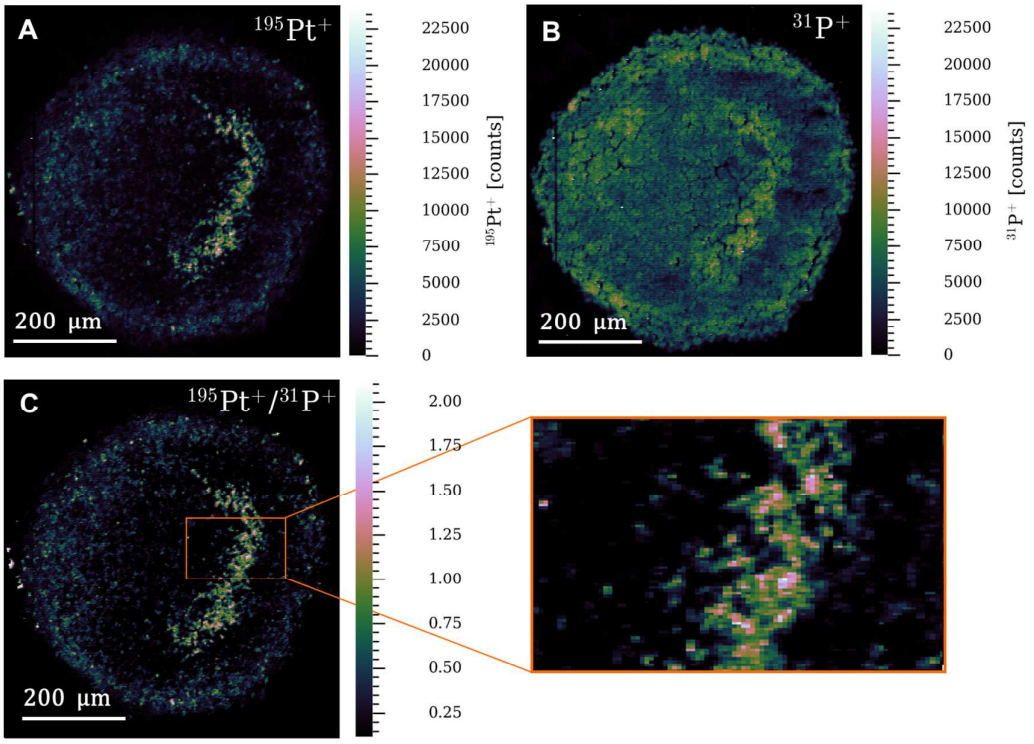

Figure 2. High-resolution LA-ICP-MS images of the (A) ^{195}Pt, (B) ^{31}P and (C) $^{195}Pt^+/^{31}P^+$ signal ratio distribution in a selected colon cancer HCT116 tumor spheroid section 2, after treatment with oxaliplatin for 24 h. The inset of Figure (C) shows a zoomed-in section of the image.

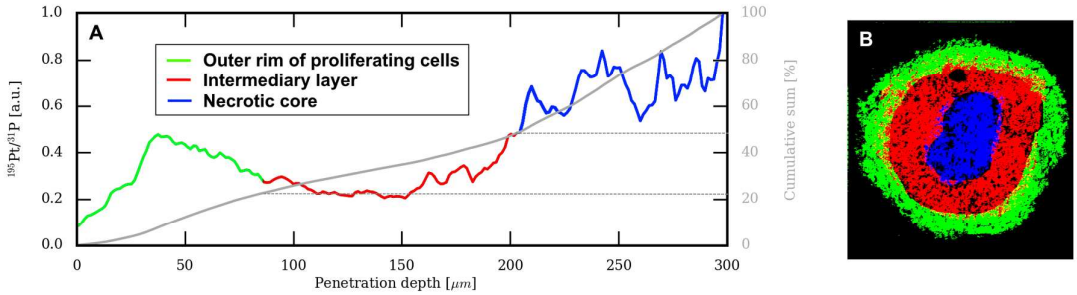

Figure 3. Visual representation of the drug penetration within the MCTS, (A) average radial profile of the $^{195}Pt^+/^{31}P^+$ signal ratio relative to the core-rim distance (the penetration depth). Three distinct zones can be differentiated, as displayed in Figure (B).

Conclusions

The use of spheroid technologies for anti-cancer drug screening regimens provides significant improvement over conventional 2D cell-based assays, when characterized properly as they more accurately reflect the reality of cellular conditions in tumors. Therefore, we showed the potential of a low dispersion LA-ICP-MS setup including the ARIS system to increase the spatial resolution of elemental imaging in tumor spheroids, as well as the speed of analysis. Phosphorus was shown to be able to compensate for variations in cell density and tissue thickness. The use of Pt/P ratios together with the high spatial resolution of ~2.5 µm adopted in this study allowed the elimination of intracellular space and the analysis of platinum accumulation in the different cell regions (proliferating, quiescent and necrotic cells) of the spheroid. This approach allows investigating the impact of platinum incorporation in different cells on the efficacy of metal-based drugs and can serve as selection criteria for drug candidates on pre-clinical stage. As the performance characteristics of this analytical setup can significantly improve the sample throughput for pre-clinical applications when using LA-ICP-MS, it can be further used to screen the uptake of different metal-based anti-cancer drugs into multicellular tumor spheroids and tumor tissue in a high-throughput manner.

Acknowledgements

We are thankful to Anastasiya Svirkova for preparing the sections of the tumor spheroid samples. The authors acknowledge financial and logistic support from the Flemish Research Foundation (FWO, research project G017217N) and Teledyne

CETAC Technologies. A.L. was supported by the Austrian Science Fund (FWF) through the project P27749. Van Malderen, S.J.M. is a Ph.D. fellow of the FWO.

References

(1) Mehta, G.; Hsiao, A. Y.; Ingram, M.; Luker, G. D.; Takayama, S. *J. Control. Rel.* **2012**, *164*, 192-204.

(2) Minchinton, A. I.; Tannock, I. F. *Nat. Rev. Cancer* **2006**, *6*, 583-592.

(3) Nath, S.; Devi, G. R. *Pharmacol. Ther.* **2016**, *163*, 94-108.

(4) Hirschhaeuser, F.; Menne, H.; Dittfeld, C.; West, J.; Mueller-Klieser, W.; Kunz-Schughart, L. A. *J. Biotechnol.* **2010**, *148*, 3-15.

(5) Liu, X.; Hummon, A. B. *Anal Chem* **2015**, *87*, 9508-9519.

(6) Bryce, N. S.; Zhang, J. Z.; Whan, R. M.; Yamamoto, N.; Hambley, T. W. *Chem. Comm.* **2009**, 2673-2675.

(7) Zhang, J. Z.; Bryce, N. S.; Lanzirotti, A.; Chen, C. K. J.; Paterson, D.; de Jonge, M. D.; Howard, D. L.; Hambley, T. W. *Metallomics* **2012**, *4*, 1209-1217.

(8) Liu, X.; Hummon, A. B. *Sci Rep* **2016**, *6*, 38507.

(9) Lee, R. F. S.; Theiner, S.; Meibom, A.; Koellensperger, G.; Keppler, B. K.; Dyson, P. J. *Metallomics* **2017**, *9*, 365-381.

(10) Zhang, J. Z.; Bryce, N. S.; Siegele, R.; Carter, E. A.; Paterson, D.; de Jonge, M. D.; Howard, D. L.; Ryan, C. G.; Hambley, T. W. *Integr. Biol.* **2012**, *4*, 1072-1080.

(11) Theiner, S.; Schreiber-Brynzak, E.; Jakupec, M. A.; Galanski, M.; Koellensperger, G.; Keppler, B. K. *Metallomics* **2016**, *8*, 398-402.

(12) Schreiber-Brynzak, E.; Pichler, V.; Heffeter, P.; Hanson, B.; Theiner, S.; Lichtscheidl-Schultz, I.; Kornauth, C.; Bamonti, L.; Dhery, V.; Groza, D.; Berry, D.; Berger, W.; Galanski, M.; Jakupec, M. A.; Keppler, B. K. *Metallomics* **2016**, *8*, 422-433.

(13) Niehoff, A.-C.; Grünebaum, J.; Moosmann, A.; Mulac, D.; Söbbing, J.; Niehaus, R.; Buchholz, R.; Kröger, S.; Wiehe, A.; Wagner, S.; Sperling, M.; von Briesen, H.; Langer, K.; Karst, U. *Anal. Chim. Acta* **2016**, *938*, 106-113.

(14) Van Malderen, S. J. M.; Managh, A. J.; Sharp, B. L.; Vanhaecke, F. *J Anal At Spectrom* **2016**, *31*, 423-439.

(15) Gundlach-Graham, A.; Günther, D. *Anal Bioanal Chem* **2016**, *408*, 2687-2695.

(16) Van Acker, T.; Van Malderen, S. J. M.; Van Heerden, M.; McDuffie, J. E.; Cuyckens, F.; Vanhaecke, F. *Anal. Chim. Acta* **2016**, *945*, 23-30.

(17) Carlier, C.; Laforce, B.; Van Malderen, S. J. M.; Gremonprez, F.; Tucoulou, R.; Villanova, J.; De Wever, O.; Vincze, L.; Vanhaecke, F.; Ceelen, W. *J. Pharm. Biomed. Anal.* **2016**, *131*, 256-262.

(18) Van Malderen, S. J. M.; Van Elteren, J. T.; Vanhaecke, F. *J. Anal. At. Spectrom.* **2015**, *30*, 119-125.

(19) Legin, A. A.; Schintlmeister, A.; Jakupec, M. A.; Galanski, M.; Lichtscheidl, I.; Wagner, M.; Keppler, B. K. *Chem Sci* **2014**, *5*, 3135-3143.

(20) Habala, L.; Galanski, M.; Yasemi, A.; Nazarov, A. A.; von Keyserlingk, N. G.; Keppler, B. K. *Eur. J. Med. Chem.* **2005**, *40*, 1149-1155.

(21) Van Malderen, S. J. M.; Van Elteren, J. T.; Vanhaecke, F. *Anal. Chem.* **2015**, *87*, 6125-6132.

(22) Wheate, N. J.; Walker, S.; Craig, G. E.; Oun, R. *Dalton Trans.* **2010**, *39*, 8113-8127.

(23) Thoma, C. R.; Zimmermann, M.; Agarkova, I.; Kelm, J. M.; Krek, W. *Adv. Drug Deliver. Rev.* **2014**, *69–70*, 29-41.

(24) Schreiber-Brynzak, E.; Klapproth, E.; Unger, C.; Lichtscheidl-Schultz, I.; Göschl, S.; Schweighofer, S.; Trondl, R.; Dolznig, H.; Jakupec, M.; Keppler, B. *Invest. New Drugs* **2015**, *33*, 835-847.

(25) Theiner, S.; Kornauth, C.; Varbanov, H. P.; Galanski, M.; Van Schoonhoven, S.; Heffeter, P.; Berger, W.; Egger, A. E.; Keppler, B. K. *Metallomics* **2015**, *7*, 1256-1264.